Mass transfer from a finite strip near an oscillating stagnation point — implications for atherogenesis

Matthias Heil and Andrew L. Hazel
Department of Mathematics, University of Manchester, Oxford Road, Manchester, M13 9PL, UK

.

In print in: Journal of Engineering Mathematics
(December 2003)

.

Abstract. We consider the mass transfer from a finite-length strip near a two-dimensional, oscillating stagnation-point flow in an incompressible, Newtonian fluid. The problem is investigated using a combination of asymptotic and numerical methods. The aim of the study is to determine the effect of the location of the strip, relative to the time-averaged position of the stagnation point, on the mass transfer into the fluid. The study is motivated by the problem of mass transfer from an injured region of the arterial wall into the blood, a process that may be of considerable importance in atherogenesis. For physiologically realistic parameter values, we find that the fluid flow is quasi-steady, but the mass transfer exhibits genuine time-dependence and a high-frequency asymptotic solution provides an accurate prediction of the time-average mass transfer. In this regime, there is a significant reduction in mass transfer when the centre of the strip is located at the point of zero time-averaged wall shear rate, or equivalently wall shear stress, which may serve to explain, at least partially, the correlation between arterial disease and regions of low wall shear stress.

1. Introduction

It is generally acknowledged that the development of diseases such as intimal hyperplasia and atherosclerosis are strongly affected by the temporal and spatial distribution of the shear stress exerted on the arterial walls by the movement of the blood. Sites that are exposed to low wall shear stress, such as those near stagnation points, appear to be particularly prone to the development of such diseases [1–3]. In the cardiovascular system, stagnation points occur naturally near the re-attachment lines of regions of separated flow (e.g., in the carotid sinus and downstream of stenoses), but may also be located opposite end-to-side anastomoses introduced into the system as a consequence of arterial bypass surgery. The pulsatile blood flow through the arteries not only causes an oscillation in the magnitude of the incoming velocity (strength), but also causes oscillations in the spatial location of such stagnation points.

Hazel and Pedley [4] considered a simple model of a spatially-oscillating stagnation-point flow and found that the interaction between the oscillations in position and strength could led to a displacement of the point of zero *mean* wall shear stress away from the centre of positional oscillations: an effect analogous to acoustic, or steady, streaming. The change in the mean wall-shear-stress distribution, caused by the introduction of time-dependence in the flow, lead Hazel and Pedley [4] to conclude that the effects of time-dependence on atherogenesis could still be a consequence of the mean, as opposed to the time-varying, component of the wall shear stress.

A vital, and as yet unresolved, step in the link between mechanics and disease is the mechanism by which the wall shear stress is translated into a biological response. Indeed, it is unclear whether the shear stress is directly responsible for the progression of disease or is merely a secondary variable that happens to be well-correlated with other processes. For example, Caro *et al.* [1] proposed a mass-transfer-based mechanism for the development of atherosclerosis. However, recent

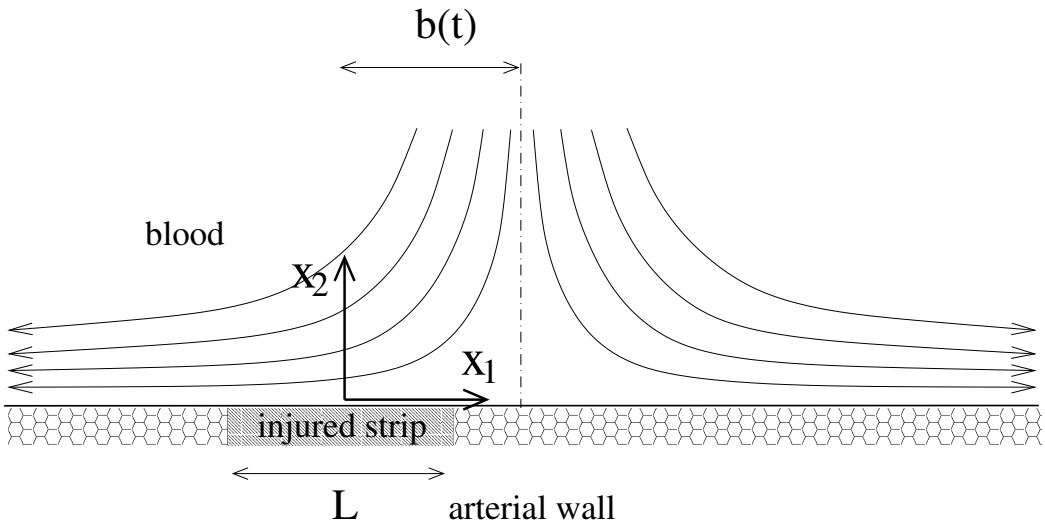

Figure 1. Sketch of the model problem. A two-dimensional stagnation-point flow performs positional oscillations, $b(t)$, in the x_1-direction and impinges onto the plane $x_2 = 0$, which represents a model of an artery wall. A short section of the wall of length L is injured and releases a chemical species into the blood.

research has demonstrated that the endothelial cells, which line the arterial walls, can act as force transducers, converting mechanical stresses into biological events, see reference [5]. These findings lend support to the idea that the wall shear stress could be the primary stimulus for disease. Nevertheless, it is still possible that passive mechanics, rather than any active response on the part of the cells, may play a rôle in disease localisation.

In this paper, we shall investigate the latter hypothesis by extending the model of Hazel and Pedley [4] to consider the effects of mass transport near an oscillating stagnation point. The idea is to simulate a region in which the arterial wall is "damaged" and secretes a generic chemical species that could activate and/or act as a chemoattractant for circulating blood components. Examples of such chemicals include adenosine diphosphate and thrombaxane A_2, both of which can activate platelets; and platelet-activating factor, an ether phospholipid, which can activate both platelets and leukocytes and acts as a chemoattractant for leukocytes; see the review [6]. We assume that the cellular response is independent of both position and wall shear stress and examine the effects of the location of the damaged region, relative to the time-average position of the stagnation point, upon the local mass transfer. If the mass transport properties are significantly different in the vicinity of a stagnation point then this mechanism, rather than any active response of the wall to shear stress, might serve to explain the correlation between disease and regions of low wall shear stress.

2. The model

We consider the transport of a chemical species, with concentration field $c^*(x_i^*, t^*)$, in a highly-idealised two-dimensional flow field, where x_i^*, $i = 1, 2$ are Cartesian coordinates and t^* is time. Throughout this paper, asterisks are used to distinguish dimensional quantities from their dimensionless equivalents. An incompressible, Newtonian fluid of kinematic viscosity ν occupies the half-plane $x_2^* > 0$, $-\infty < x_1^* < \infty$ and an unsteady, two-dimensional stagnation-point flow impinges onto a plane, impermeable wall at $x_2^* = 0$; see figure 1. The inviscid, far-field ($x_2^* \to \infty$) velocity field is given

by

$$u_1^* = A(t^*)\ (x_1^* - b^*(t^*)) \quad \text{and} \quad u_2^* = -A(t^*)\ x_2^*, \tag{1}$$

where u_i^* is the velocity component in the x_i^*-direction. Here, the strength of the stagnation-point flow varies sinusoidally in time, t^*, about a mean value A_0 with relative amplitude α

$$A(t^*) = A_0\,(1 + \alpha\ \sin(2\pi t^*/T))\,. \tag{2}$$

Additionally, the location of the stagnation point oscillates about a mean position $x_1^* = b_0^*$ with amplitude b_1^*

$$b^*(t^*) = b_0^* + b_1^* \sin(2\pi t^*/T + \phi)\,. \tag{3}$$

We assume that the period, T, of the two oscillations is the same, as might be expected in the cardiovascular system, but allow for a phase difference, ϕ. Provided that the period of the oscillation is sufficiently large, there is a quasi-steady velocity boundary layer of thickness $\delta_{stag} = \mathcal{O}(\sqrt{\nu/A})$ near the wall, in which the velocity is given by

$$u_1^* = A(t^*)\ (x_1^* - b^*(t^*))\ f'\left(x_2^*\sqrt{\frac{A(t^*)}{\nu}}\right) \quad \text{and} \quad u_2^* = -\sqrt{\nu A(t^*)}\ f\left(x_2^*\sqrt{\frac{A(t^*)}{\nu}}\right). \tag{4}$$

f is a solution of the ordinary differential equation

$$f''' + ff'' + 1 - f'^2 = 0, \tag{5}$$

with the boundary conditions $f(0) = f'(0) = 0$ and $f'(\infty) = 1$; see, e.g., reference [7 , pp. 152–157].

The diffusivity, D, of thrombogenic factors in blood is generally rather small, leading to large values of the Schmidt number, $Sc \equiv \nu/D$, and it follows that the concentration boundary layer will be much thinner than the stagnation-point boundary layer. We therefore approximate the velocity field within the concentration boundary layer by linearising (4) for small $Y = x_2^*\sqrt{A(t^*)/\nu}$, giving

$$u_1^* = \frac{A_0^{3/2}}{\nu^{1/2}} f''(0)(1 + \alpha\ \sin(2\pi t^*/T))^{3/2}(x_1^* - b^*(t^*))x_2^*, \tag{6a}$$

$$u_2^* = -\frac{1}{2}\frac{A_0^{3/2}}{\nu^{1/2}} f''(0)(1 + \alpha\ \sin(2\pi t^*/T))^{3/2}x_2^{*2}, \tag{6b}$$

where $f''(0) \approx 1.23259$; see reference [7, p 157].

We choose the coordinate system such that the region of injury is located in a strip of length L, centred at the origin. The most appropriate wall boundary condition is probably a mixed condition of the form

$$a_1 c^* + a_2 \frac{\partial c^*}{\partial x_2^*} = a_3, \tag{7}$$

but the choice of the coefficients a_i is far from obvious. A first attempt is to assume that the concentration is fixed over the damaged region and that the undamaged region remains passive and impermeable to the chemical: i.e. $c^* \equiv c_0$ for $x_2^* = 0$, $-L/2 < x_1^* < L/2$ and $\partial c^*/\partial x_2^* = 0$ otherwise. This assumption corresponds to the case in which all the wall binding sites for the chemical are occupied and the reaction kinetics are sufficiently fast that any empty sites are reoccupied instantly. Far away from the strip the concentration approaches a uniform background level, $c^* \to c_\infty$ as $x_2^* \to \infty$.

We non-dimensionalise by letting $x_i^* = x_i(L/2)$, $b^* = b(L/2)$, $t^* = tT$, $c^* = c_\infty + c(c_0 - c_\infty)$ and $\mathbf{u}^* = U_0\mathbf{u}$, where U_0 is the appropriate scale for the quasi-steady

flow in the linearised stagnation-point boundary layer (6a,b),

$$U_0 = \frac{A_0^{3/2} f''(0) L^2}{4\nu^{1/2}}. \tag{8}$$

In this non-dimensionalisation, the advection-diffusion equation, which governs the concentration of the chemical species, becomes

$$Pe_0 \left(St\ \frac{\partial c}{\partial t} + u_1 \frac{\partial c}{\partial x_1} + u_2 \frac{\partial c}{\partial x_2} \right) = \frac{\partial^2 c}{\partial x_1^2} + \frac{\partial^2 c}{\partial x_2^2}, \tag{9}$$

where

$$u_1 = (1 + \alpha\ \sin(2\pi t))^{3/2} (x_1 - b(t)) x_2 \ \text{ and } \ u_2 = -\frac{1}{2}(1 + \alpha\ \sin(2\pi t))^{3/2} x_2^2, \tag{10}$$

and the boundary conditions are

$$c = 1 \quad \text{for } x_2 = 0 \text{ and } |x_1| < 1, \tag{11a}$$

$$\frac{\partial c}{\partial x_2} = 0 \quad \text{for } x_2 = 0 \text{ and } |x_1| > 1, \tag{11b}$$

$$c \to 0 \quad \text{as } x_2 \to \infty. \tag{11c}$$

The Péclet number, Pe_0, reflects the ratio of the time-scales for advective and diffusive transport, whereas the Strouhal number, St, is the ratio of the time-scale for advective transport to the period of the stagnation-point oscillations:

$$Pe_0 \equiv \frac{U_0 L}{2D} = \frac{A_0^{3/2} f''(0) L^3}{8 D \nu^{1/2}} \quad \text{and} \quad St \equiv \frac{L}{2 U_0 T} = \frac{2\nu^{1/2}}{T A_0^{3/2} f''(0) L}. \tag{12}$$

The aim of the analysis is to determine the concentration field $c(x_i, t)$ and the total mass flux from the strip into the blood stream, $Q^* = -D \int_{-L/2}^{L/2} \partial c^* / \partial x_2^*\ \mathrm{d}x_1^*$. A dimensionless form of the mass flux is given by the Sherwood number

$$Sh = \frac{Q^*}{D(c_0 - c_\infty)} = -\int_{-1}^{1} \frac{\partial c}{\partial x_2}\ \mathrm{d}x_1, \tag{13}$$

and we denote its long-time average by $\overline{Sh}$, where, given any function, $F(t)$,

$$\overline{F} \equiv \lim_{\tau \to \infty} \int_{\tau}^{\tau+1} F(t)\ \mathrm{d}t. \tag{14}$$

For later reference we note that the dimensionless wall shear stress is given by

$$\tau(t, x_1) = \frac{\tau^*(t^*, x_1^*)}{2\mu U_0 / L} = \frac{\partial u_1}{\partial x_2} = (1 + \alpha\ \sin(2\pi t))^{3/2} (x_1 - b(t)), \tag{15}$$

and the spatially-averaged wall shear stress over the strip is

$$\tau_{\mathrm{av}}(t) = \frac{1}{2} \int_{-1}^{1} \tau(t, x_1)\ \mathrm{d}x_1 = -b(t)\ (1 + \alpha\ \sin(2\pi t))^{3/2}. \tag{16}$$

Furthermore, the x_1-position at which the time-averaged wall shear stress is zero is given by

$$x_1^{\overline{\tau}=0} = \frac{\overline{b(t)(1 + \alpha \sin(2\pi t))^{3/2}}}{\overline{(1 + \alpha \sin(2\pi t))^{3/2}}} = \frac{-\overline{\tau_{\mathrm{av}}}}{\overline{(1 + \alpha \sin(2\pi t))^{3/2}}} = b_0 + b_1 \mathcal{F}(\alpha) \cos(\phi), \tag{17}$$

where $\mathcal{F}(\alpha)$ may be expressed in terms of elliptic integrals.

3. Analysis

3.1. Quasi-steady analytic approximations

In the limit $St \to 0$, the solution becomes quasi-steady and $c(x_i, t)$ is given, to leading order, by the steady solution corresponding to the instantaneous values of the stagnation-point offset, $b(t)$, and the Péclet number, $Pe = Pe_0\ (1 + \alpha \sin(2\pi t))^{(3/2)}$. We further assume that Pe is sufficiently large that we may neglect horizontal diffusion — a boundary-layer approximation.

3.1.1. *$Pe \gg 1$ and $|b| \ll 1$*

Firstly, we consider the case in which the stagnation point is located near the centre of the strip, $|b| \ll 1$. As the length of the strip increases, $L \to \infty$ or equivalently $Pe \to \infty$, we expect the concentration field to become independent of x_1, apart from small regions near the ends of the strip. In this case, the governing equation (9) reduces to an ordinary differential equation

$$\frac{d^2c}{d\zeta^2} + 3\zeta^2 \frac{dc}{d\zeta} = 0, \tag{18}$$

where the rescaling $x_2 = (Pe/6)^{-1/3}\zeta$ has been used to eliminate the Péclet number. The solution, subject to the boundary conditions

$$c(0) = 1 \quad \text{and} \quad c(\infty) = 0, \tag{19}$$

is given by

$$c(\zeta) = 1 - \frac{1}{\Gamma(4/3)} \int_0^\zeta e^{-\kappa^3}\ \mathrm{d}\kappa. \tag{20}$$

Hence, the dimensionless flux over the strip is

$$Sh_{|b|\ll 1} = -\left(\frac{Pe}{6}\right)^{1/3} \int_{-1}^{1} \left.\frac{dc}{d\zeta}\right|_{\zeta=0} \mathrm{d}x_1 = \frac{2}{\Gamma(4/3)}\ \left(\frac{Pe}{6}\right)^{1/3} \approx 1.2335\ Pe^{1/3}. \tag{21}$$

3.1.2. *$Pe \gg 1$ and $|b| \gg 1$*

If the stagnation point is far away from the strip, $|b| \gg 1$ (without loss of generality we shall assume that $b > 0$), we expect the behaviour to be similar to that of a uniform shear flow over the strip. We introduce a coordinate X measured from the upstream end of the strip, $x_1 = 1 - X$, and rescale the transverse coordinate by $x_2 = b^{-1/3}\eta$. The governing equation (9) becomes

$$Pe\ \eta\ \frac{\partial c}{\partial X} = \frac{\partial^2 c}{\partial \eta^2} + \mathcal{O}(b^{-2/3}). \tag{22}$$

In the limit, $b \to \infty$, equation (22) is indeed equivalent to that derived in Leveque's uniform shear theory [8]. Following Leveque's analysis [8] we introduce the similarity variable

$$\zeta = \left(\frac{1}{9}\right)^{1/3} \eta\ X^{-1/3}\ Pe^{1/3}, \tag{23}$$

whereupon (22) becomes (18), again subject to the boundary conditions (19). Thus, (20) is also the solution for the present problem, but here the flux is given by

$$\left.\frac{\partial c}{\partial x_2}\right|_{x_2=0} = -\frac{1}{\Gamma(4/3)} \left(\frac{b\ Pe}{9}\right)^{1/3} (1 - x_1)^{-1/3}. \tag{24}$$

The total flux is

$$Sh_{|b|\gg 1} = -\int_{-1}^{1} \left.\frac{\partial c}{\partial x_2}\right|_{x_2=0} \mathrm{d}x_1 = \frac{1}{\Gamma(4/3)}\left(\frac{3}{2}\right)^{1/3} (|b|\ Pe)^{1/3} \approx 1.2819\ (|b|\ Pe)^{1/3}, \tag{25}$$

where we have generalised the result to include the case $b < 0$. Recalling that $Pe = Pe_0(1 + \alpha \sin(2\pi t))^{3/2} > 0$, equation (25) demonstrates that the mass flux is proportional to the instantaneous value of the cube-root of the spatially-averaged wall shear stress over the strip, $|\tau_{\mathrm{av}}|^{1/3}$, see equation (16), as in the uniform shear theory.

3.2. Large Strouhal number asymptotic expansion

At finite Strouhal numbers, the time-derivative in the governing equation (9) can no longer be neglected, and we now derive an asymptotic approximation for the time-periodic solutions in the limit $St \to \infty$. We first consider the case in which the stagnation point is always located at a large distance from the strip. In terms of the coordinate $X = 1 - x_1$ and the steady boundary-layer similarity variable $\zeta = [Pe_0\ b_0/(9X)]^{1/3} x_2$, introduced in §3.1.2, equation (9) becomes

$$\left(\frac{9X}{b_0}\right)^{2/3} Pe_0^{1/3} St \frac{\partial c}{\partial t} = \frac{\partial^2 c}{\partial \zeta^2} + \Omega(t)\left\{3\zeta^2 \frac{\partial c}{\partial \zeta} - 9X\zeta \frac{\partial c}{\partial X}\right\} + \mathcal{O}(X/b_0) + \mathcal{O}(Pe_0^{-2/3}), \tag{26}$$

where

$$\Omega(t) = (1 + \alpha \sin(2\pi t))^{(3/2)}(1 + (b_1/b_0)\sin(2\pi t + \phi)). \tag{27}$$

It is apparent, that the dimensionless combination

$$\chi = \left(\frac{9X}{b_0}\right)^{2/3} Pe_0^{1/3} St,$$

governs the relative importance of time-dependence in the problem, with $\chi \to \infty$ being the limit of high Strouhal number. As $\chi \to \infty$, the highest order spatial derivatives in equation (26) become small compared to the time derivative and we use the method of matched asymptotic expansions to investigate this singular limit. The appropriate inner solution must represent a balance between the highest order spatial derivative and the time-derivative and the inner variable is thus

$$\xi = \chi^{1/2}\zeta = (Pe_0\ St)^{1/2} x_2 = x_2^*/\sqrt{TD}, \tag{28}$$

which represents a rescaling of the wall-normal coordinate on the thickness, $\sqrt{TD}$, of a concentration "Stokes" layer. The following analysis closely follows that of Pedley [9], the difference being that he used the simpler function $\Omega(t) = 1 + \alpha \sin(2\pi t)$.

3.2.1. *Outer solution*

In the outer region, we recast equation (9) in terms of the variables (χ, ζ) to obtain

$$\frac{\partial c}{\partial t} = \chi^{-1}\left[\frac{\partial^2 c}{\partial \zeta^2} + \Omega(t)\left\{3\zeta^2 \frac{\partial c}{\partial \zeta} - 6\chi\zeta \frac{\partial c}{\partial \chi}\right\}\right], \tag{29}$$

where we assume that $Pe_0 \gg 1$, $b_0 \gg 1$ and $\Omega(t) > 0$. The latter condition requires that $\alpha < 1$, $b_1 < b_0$; if these conditions are violated then $\Omega(t)$ passes through zero during the cycle and at these instants the advective terms become negligible causing the present approximation to break down. The boundary conditions are that $c \to 0$ as $\zeta \to \infty$ and that the solution must match onto the inner solution as $\zeta \to 0$. We pose the series expansion

$$c = \sum_{n=0}^{\infty} \chi^{-n/2} \tilde{c}_n(\zeta, t),$$

and after substitution into equation (29) and equating like powers of χ, the first three equations are:

$$\frac{\partial \tilde{c}_0}{\partial t} = 0, \quad \frac{\partial \tilde{c}_1}{\partial t} = 0, \quad \text{and} \quad \frac{\partial \tilde{c}_2}{\partial t} = \frac{\partial^2 \tilde{c}_0}{\partial \zeta^2} + \Omega(t)\ 3\zeta^2 \frac{\partial \tilde{c}_0}{\partial \zeta}. \tag{30}$$

The first equation implies that $\tilde{c}_0$ is a function of ζ only and the secularity condition for $\tilde{c}_2$ further implies that

$$\int_0^1 \left[\frac{\partial^2 \tilde{c}_0}{\partial \zeta^2} + \Omega(t)\ 3\zeta^2 \frac{\partial \tilde{c}_0}{\partial \zeta} \right] \mathrm{d}t = \frac{\partial^2 \tilde{c}_0}{\partial \zeta^2} + \int_0^1 \Omega(t)\mathrm{d}t\ 3\zeta^2 \frac{\partial \tilde{c}_0}{\partial \zeta} = 0, \tag{31}$$

which is, yet again, equation (18), after a suitable change of variables. $\tilde{c}_0$ must satisfy the boundary condition at infinity and the additional condition that c must approach the steady solution when $\alpha = b_1 = 0$; hence,

$$\tilde{c}_0 = (1 + a_0\ g(\alpha, b_1, \phi)) \left(1 - \frac{1}{\Gamma(4/3)} \int_0^{\zeta \overline{\Omega}^{\frac{1}{3}}} e^{-\kappa^3}\ \mathrm{d}\kappa \right),$$

where $\overline{\Omega} = \int_0^1 \Omega(t)\mathrm{d}t$, a_0 is an unknown constant and $g(\alpha, b_1, \phi)$ is an unknown function that must be zero when $\alpha = b_1 = 0$.

3.2.2. *Inner solution*

In terms of the inner variables (χ, ξ), equation (9) becomes

$$\frac{\partial^2 c}{\partial \xi^2} - \frac{\partial c}{\partial t} = \chi^{-1/2}\ \Omega(t)\ 6\xi \frac{\partial c}{\partial \chi}, \tag{32}$$

again assuming that $Pe_0 \gg 1$, $|b| \gg 1$ and $\alpha < 1$. The boundary conditions are that $c = 1$ at $\xi = 0$ and that the solution matches to the outer solution, as $\xi \to \infty$. We pose the series expansion

$$c = \sum_{n=0}^{\infty} \chi^{-n/2} \hat{c}_n(\xi, t),$$

and the first two equations are

$$\frac{\partial^2 \hat{c}_0}{\partial \xi^2} - \frac{\partial \hat{c}_0}{\partial t} = 0, \quad \text{and} \quad \frac{\partial^2 \hat{c}_1}{\partial \xi^2} - \frac{\partial \hat{c}_1}{\partial t} = 0. \tag{33}$$

At leading order, the boundary conditions are

$$\hat{c}_0(0, t) = 1, \quad \text{and} \quad \hat{c}_0(\infty, t) = 1 + a_0 g(\alpha, b_1, \phi).$$

Equation (33a) is an unsteady heat equation and does not have any non-trivial time-periodic solutions. For a time-periodic solution, therefore, $a_0 = 0$, in which case the leading order inner solution is a constant, $\hat{c}_0 \equiv 1$. Hence, in order to calculate the mass transfer at leading order, we need the next order term in the inner expansion. The boundary conditions are

$$\hat{c}_1(0, t) = 0, \quad \text{and} \quad \hat{c}_1(\xi, t) \sim -\overline{\Omega}^{1/3}/\Gamma(4/3)\xi + \tilde{c}_1(0) \quad \text{as } \xi \to \infty.$$

Again, only the trivial time-periodic solution is possible, in which case $\tilde{c}_1(0) \equiv 0$ and

$$\hat{c}_1 = -\overline{\Omega}^{1/3}/\Gamma(4/3)\xi.$$

The leading-order concentration gradient at the wall is then

$$\left.\frac{\partial c}{\partial x_2}\right|_{x_2=0} = \left(\frac{b_0\ Pe_0}{9}\right)^{1/3} (1-x_1)^{-1/3} \chi^{1/2}\ \left.\frac{\partial c}{\partial \xi}\right|_{\xi=0} = -\frac{\overline{\Omega}^{1/3}}{\Gamma(4/3)} \left(\frac{b_0\ Pe_0}{9}\right)^{1/3} (1-x_1)^{-1/3}. \tag{34}$$

It follows that in the limit $St \to \infty$, $|b| \gg 1$, the concentration near the wall becomes independent of time and the instantaneous and time-average mass transfer is

$$Sh_{|b|\gg 1} = \overline{Sh}_{|b|\gg 1} \approx 1.2819\ (|b_0\overline{\Omega}|\ Pe_0)^{1/3} = 1.2819\ (|\overline{\tau_{\rm av}}|\ Pe_0)^{1/3}. \qquad (35)$$

A similar analysis carries through in the case when $|b| \ll 1$ and, by analogy with the quasi-steady results, §3.1, the leading order contribution to the mass transfer is

$$Sh_{|b|\ll 1} = \overline{Sh}_{|b|\ll 1} \approx 1.2335\ \left(\ \overline{(1+\alpha\sin(2\pi t))^{3/2}}\ Pe_0\right)^{1/3}. \qquad (36)$$

3.3. Numerical Solution

The analysis presented above applies in the limits of large and small Strouhal numbers. For intermediate values of St, equation (9) must be solved numerically. For this purpose we approximate the upper half plane by the finite rectangle $-L_1 \le x_1 \le L_1$, $0 \le x_2 \le L_2$ and apply the far-field boundary condition (11c) at $x_2 = L_2$. We apply the wall boundary conditions (11a,11b) at $x_2 = 0$ and impose $\partial c/\partial n = 0$ along the edges $x_1 = \pm L_1$, corresponding to passive advection out of the domain. The domain is decomposed into nine-node quadrilateral finite elements, with a greater concentration of elements near the wall and the ends of the strip. There is a square-root singularity in the flux at the ends of the strip (see, e.g. [10 , Appendix A]), which cannot be resolved using the standard quadratic basis functions. We therefore augment the finite-element basis by two functions which capture the appropriate singular behaviour, and approximate the concentration field, $c(x_i, t)$, by

$$c = c^{(FEM)} + \widehat{C_1}(t)\ f_1(r_1,\varphi_1) + \widehat{C_2}(t)\ f_2(r_2,\varphi_2),\ \text{where}\ \ c^{(FEM)} = \sum_{j=1}^{N} C_j(t)\psi_j. \qquad (37)$$

ψ_j are piecewise bi-quadratic finite-element shape functions, with amplitudes $C_j(t)$, $j = 1, ..., N$; r_i and φ_i $(i = 1, 2)$ are polar coordinates, centred at the two endpoints of the strip (at $x_1 = -1$ and $x_1 = +1$, respectively), and $\widehat{C_i}(t)$ are the amplitudes of the two additional functions

$$f_1 = 1 - \sqrt{r_1}\sin(\varphi_1/2) \quad \text{and} \quad f_2 = 1 - \sqrt{r_2}\cos(\varphi_2/2). \qquad (38)$$

The finite element coefficients, $C_j(t)$, not imposed by the boundary conditions are determined from the weak form of the governing equation (9),

$$f_j = \int_{-L_1}^{L_1}\int_0^{L_2} \left(Pe_0 \left(St\ \frac{\partial c}{\partial t} + u_k \frac{\partial c}{\partial x_k} \right) \psi_j + \frac{\partial c}{\partial x_k}\frac{\partial \psi_j}{\partial x_k} \right) \mathrm{d}x_1 \mathrm{d}x_2 = 0, \qquad (39)$$

where the Einstein summation convention is used and the dummy indices take the values $k = 1, 2$. Two additional equations are required to determine the amplitudes $\widehat{C_i}(t)$ and we imposed the conditions

$$\frac{\partial c^{(FEM)}}{\partial x_2} = 0 \quad \text{at } x_2 = 0 \text{ and } x_1 = \pm 1, \qquad (40)$$

ensuring that the part of the solution approximated by $c^{(FEM)}$ remains smooth throughout the domain. The time derivative was discretised by a second-order backward-Euler (BDF2) scheme and the resulting large, sparse system of algebraic equations that arises at every time step was solved using the frontal solver MA42 from the HSL2000 library.

The thickness of the concentration boundary layer changes with the Péclet number and we altered the height of the computational domain accordingly by setting $L_2 = \min(\widehat{L_2},\ \widehat{L_2}\ Pe_0^{-1/3})$, where $\widehat{L_2} = 7$ provided an adequate height for $Pe_0 = 10$;

see figure 2. The half-width of the computational domain was always $L_1 = 20$. The standard spatial resolution involved approximately 43,000 degrees of freedom. Typically, a time-step of $\Delta t = 6.25 \times 10^{-3}$ was used in the BDF2 scheme and $\overline{Sh}$ was determined by continuing the computation until $\overline{Sh}$ changed by less than 0.01% between two subsequent periods of oscillation. To validate the code, we postulated a solution for the concentration field $c(x_i, t)$ and made this an exact solution of the governing equation by adding appropriate source terms to (9) and (39). Further validation was provided by comparisons with the analytic approximations derived above. Finally, we confirmed the independence of the results on the spatial discretisation, the time step and the dimensions of the computational domain, L_1 and L_2.

4. Physiological parameter values

The period of the stagnation-point oscillation is determined by the heart rate and we take $T \approx 0.83$ sec, corresponding to a heart rate of 50 beats per minute. For a representative diffusivity of $D = 3 \times 10^{-10}$ m^2/sec (an estimated value for ADP; see reference [11]) and the viscosity of blood, $\nu \approx 4 \times 10^{-6}$ m^2/sec, we obtain a Schmidt number of $Sc = 1.33 \times 10^4$. Hazel and Pedley [4] surveyed measurements from a number of *in vivo* and *in vitro* physiological, stagnation-point flows and provided estimates for the remaining flow parameters. In the available experiments, the mean stagnation-point strength was found to lie in the range $A_0 \approx 10 - 50$ sec^{-1} and the pulsatility of the flow was estimated to be about $\alpha \approx 0.5 - 0.6$. The estimates for the phase angle varied between $\phi = -130^o$ and $\phi = -210^o$. We are concerned with the early stages of disease during which only a small section of the wall is damaged. We, therefore, choose a length-scale of $L = 3 \times 10^{-4}$ m which is comparable to the length occupied by approximately 10 endothelial cells.

Even though many of the above estimates are very crude, a number of assumptions made in the analysis appear to be justified. The Strouhal numbers are small, between 0.04 and 0.4, and Hazel and Pedley [4] found that the use of the quasi-steady boundary-layer approximation (4) was justified in this regime. Furthermore, the Schmidt number is large enough to justify the linearisation of the velocity profile in (6a,b). The Péclet numbers corresponding to the above estimates lie between 200 and 2500, which are sufficiently large for the high Péclet number analysis to apply. Nevertheless, the small length-scales in the present problem lead to relatively low values of the Péclet number, compared to those appropriate for macroscopic mass transport in the arteries.

5. Results

Despite the extreme simplicity of our model, the mass transfer still depends on six non-dimensional parameters: (i) the Strouhal number, St, (ii) the average Péclet number, Pe_0, (iii) the flow pulsatility, α, (iv) the average stagnation-point position, b_0, (v) the amplitude of positional oscillation, b_1, and (vi) the phase angle ϕ. We shall illustrate the effects of these parameters in a sequence of increasingly complex scenarios, beginning with the simplest case: steady stagnation-point flow. In all cases, we shall focus on how the location of the damaged region, relative to the average stagnation-point position, b_0, affects the mass transfer.

5.1. Steady flows

In steady stagnation-point flow $St = \alpha = b_1 = 0$, and only two parameters govern the problem, Pe and $b = b_0$. Figure 2 shows the concentration profiles at $Pe = 10$ and $Pe = 1500$, for two different stagnation-point locations, $b = 0$ and $b = -5$.

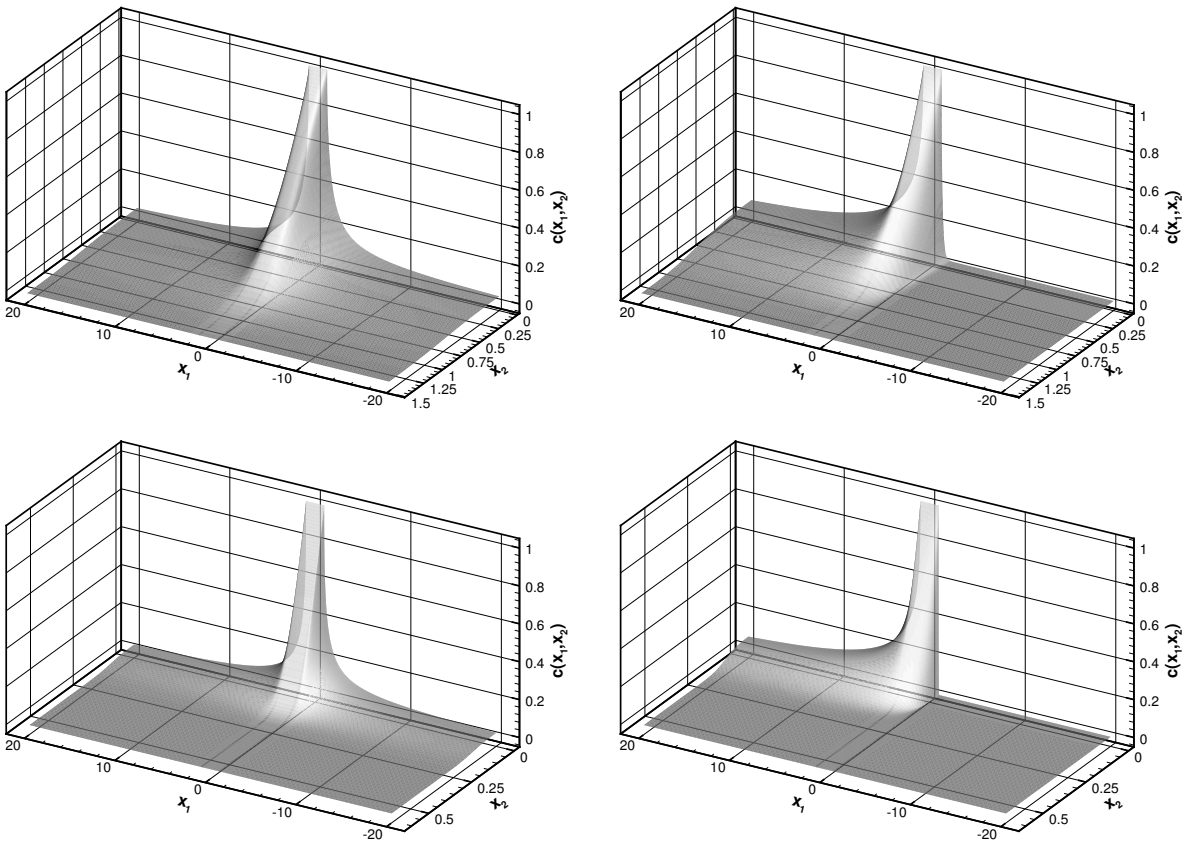

Figure 2. Steady concentration profiles, $c(x_1, x_2)$, for $b = 0$ (left column) and $b = -5$ (right column), $Pe = 10$ (top row) and $Pe = 1500$ (bottom row). Note the different ranges of the x_2-axes.

The main effect of increasing the Péclet number is to cause a relative increase in the convection towards the wall, confining the region of high concentration to a thin layer and inducing a high concentration gradient at the surface of the strip. If $b = 0$, the stagnation point is located at the centre of the strip and the solute is transported away symmetrically. If $|b| > 1$, the tangential flow above the strip is unidirectional and its magnitude increases with $|b|$, see (10). Thus, the layer of high concentration becomes strongly skewed in the direction of the dominant tangential velocity, causing the concentration gradient at the strip to increase with $|b|$.

Figure 3 illustrates the increase in dimensionless mass flux, Sh, with stagnation-point position, b, and Péclet number, Pe. The computational results (solid lines) are shown, together with the asymptotic approximations (21) and (25) for small and large b. The agreement between the numerical results and the asymptotic predictions, in their appropriate regions of validity, is very good and a global approximation for the dimensionless mass flux can be obtained by patching together the two asymptotic expressions,

$$Sh_{comp}(b, Pe) = \begin{cases} Sh_{|b|\ll 1} = 1.2335\ Pe^{1/3} & \text{for } |b| < 0.891, \\ Sh_{|b|\gg 1} = 1.2819\ (|b|\ Pe)^{1/3} & \text{for } |b| \geq 0.891. \end{cases} \tag{41}$$

5.2. Unsteady flows

In this section, we shall investigate the effects of time-dependence on both the instantaneous mass transfer, $Sh(t)$, and its time average, $\overline{Sh}$. Initially, we shall consider only oscillations in the incoming flow, §5.2.1. Next, we examine the effects of oscillations in the stagnation-point location, in the case when the incoming velocity

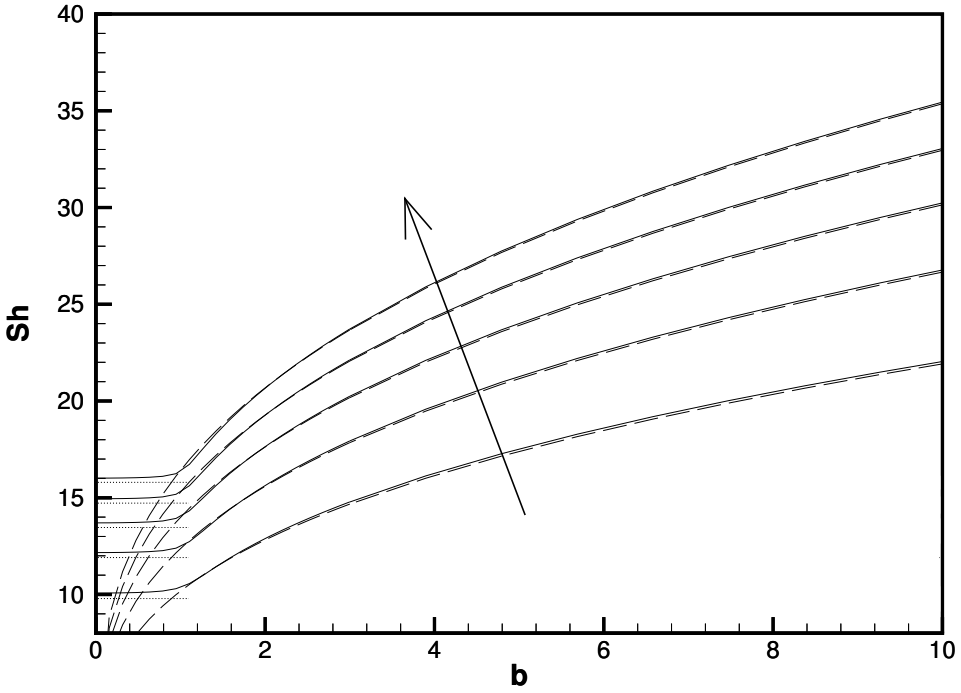

Figure 3. Non-dimensional mass flux, Sh, versus stagnation point offset, b, for steady flow. $Pe = 500, 1000, 1500, 2000, 2500$, increasing in the direction of the arrow. Solid lines: computational results; broken lines: asymptotic approximations for small b (dotted) and large b (dashed).

is steady, §5.2.2. Finally, we consider the complete problem of a stagnation-point oscillating in position and with time-varying strength, §5.2.3.

5.2.1. *Flow pulsatility*

To investigate the effect of flow pulsatility we set $b_1 = 0$ and chose $\alpha = 0.6$ as a representative value, see §4. The lower graph in figure 4 shows the strength of the incoming stagnation-point flow, as measured by the ratio $Pe/Pe_0 = (1 + \alpha \sin(2\pi t))^{(3/2)}$. The corresponding instantaneous mass transfer, $Sh(t)$, is shown on the upper graph for $St = 0$ (quasi-steady flow), $St = 0.04$, $St = 0.4$, and for two stagnation-point locations, $b_0 = 3$, $b_0 = 20$.

For $St = 0$, the analysis of §3.1 applies and the instantaneous mass transfer is well-approximated by

$$Sh(t) = Sh_{comp}(b_0, \mathrm{Pe}_0)\ (1 + \alpha \sin(2\pi t))^{(1/2)}, \tag{42}$$

shown as the dotted lines in the upper graph of figure 4. If $St \neq 0$, the introduction of "thermal" inertia causes a reduction in the amplitude of $Sh(t)$ and introduces a phase lag between $Sh(t)$ and the instantaneous stagnation-point strength, or equivalently the wall shear stress. As in the steady case, §5.1, moving the stagnation point away from the strip, increasing b_0, causes an increase in tangential advection and hence an increase in the mass transfer.

The variation of the average mass transfer, $\overline{Sh}$, with the location of the stagnation point, b_0, is shown in figure 5. For $St = 0$, $\overline{Sh}$ is slightly lower than for the corresponding steady case. The explanation for this reduction follows from the analytic solution (42), indicating that the mass transfer varies with $(1+\alpha \sin(2\pi t))^{(1/2)}$, which has a time-average slightly less than one (0.975 for $\alpha = 0.6$). An increase in St leads to a slight increase in the average mass transfer compared to the steady case; a

result following from the large-Strouhal number analysis of §3.2, which predicts that $\overline{Sh}_{St\gg 1}/\overline{Sh}_{St=0} = \left(\overline{\Omega(t)}\right)^{1/3} = 1.022$ for $\alpha = 0.6$.

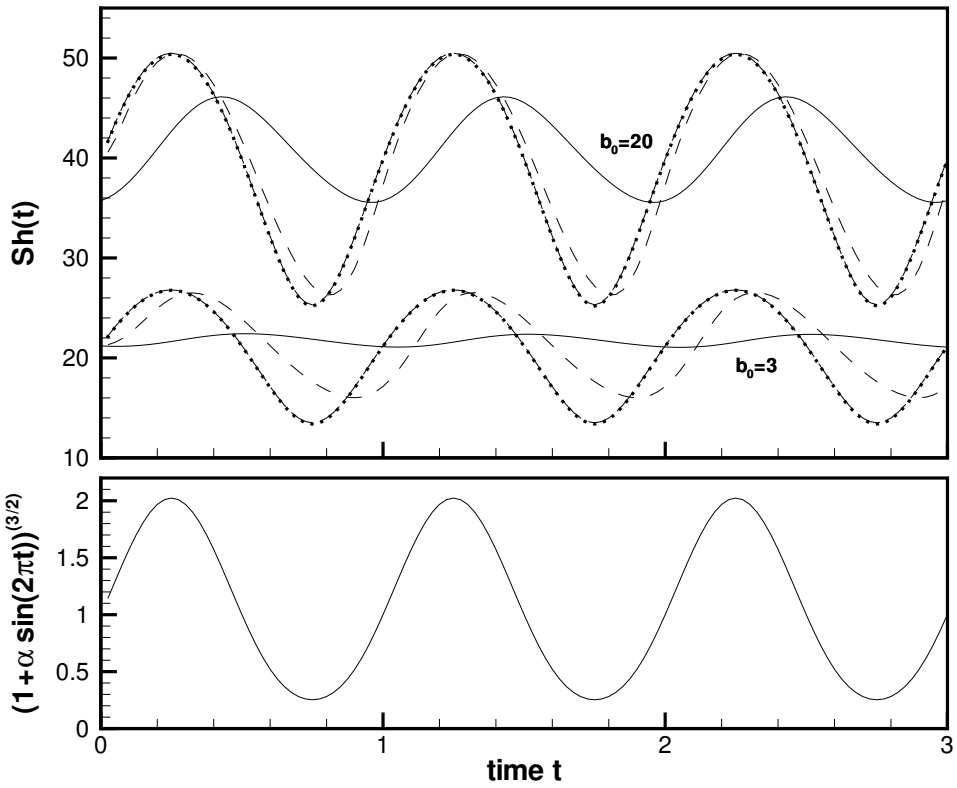

Figure 4. Upper graph: Instantaneous mass transfer $Sh(t)$ for a pulsatile stagnation point flow at two different offsets ($b_0 = 3$ and $b_0 = 20$), $Pe_0 = 1500$, $\alpha = 0.6$. Short-dashed line: $St = 0$; long-dashed line: $St = 0.04$; solid line: $St = 0.4$; dotted line: the composite approximation (42). The latter is virtually indistinguishable from the computational results for $St = 0$. Lower graph: Corresponding strength of the stagnation point flow, $Pe/Pe_0 = (1 + \alpha \sin(2\pi t))^{(3/2)}$.

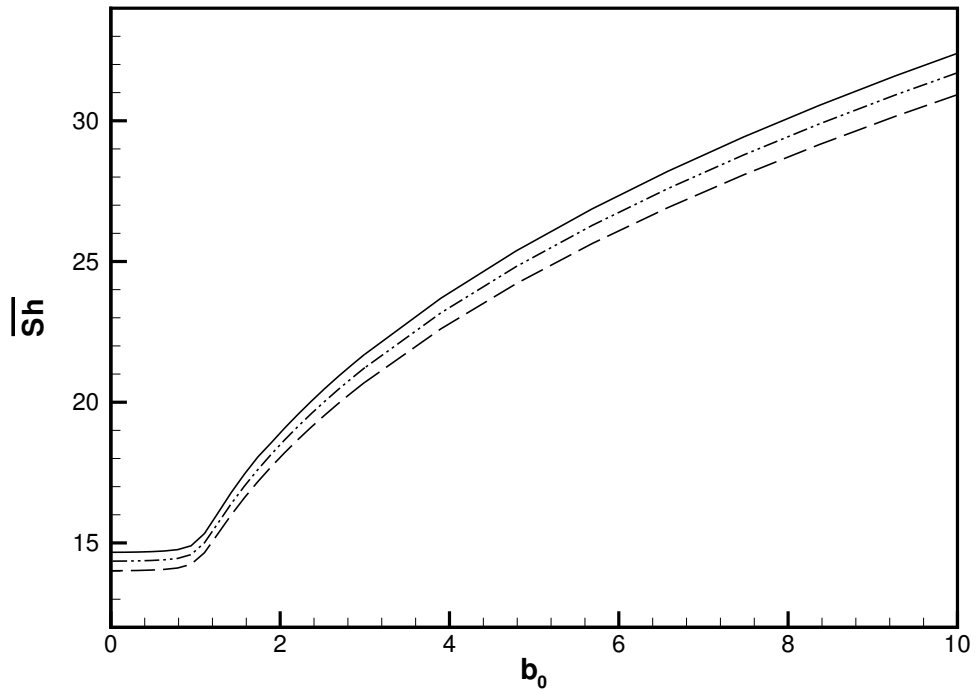

Figure 5. Average mass transfer $\overline{Sh}$ for a pulsatile stagnation point flow, $Pe_0 = 1500,\ \alpha = 0.6$. Dashed line: $St = 0$; solid line: $St = 0.4$; dash-dotted line: steady result ($\alpha = 0$).

Rescaling the results for $St = 0$ by $1/0.975$ and $St = 0.4$ by $1/1.022$ collapses the data onto the steady results with an error of less than 0.7% over the entire range of b_0 considered in figure 5. Overall, however, the effect of pure flow pulsatility on the time-average mass transfer is very small.

5.2.2. *Stagnation point motion*

We now consider steady stagnation-point flow, $\alpha = 0$, but allow the location of the stagnation point to oscillate in time, $b_1 \neq 0$. The lower graphs in figure 6 show the location of the stagnation point $b(t) = b_0 + b_1 \sin(2\pi t)$ for $b_1 = 7.5$ and two different average positions, $b_0 = -2.1$ (left) and $b_0 = -13.28$ (right). The corresponding variations in $Sh(t)$ are shown in the upper graphs for the quasi-steady case, $St = 0$, and for $St = 0.04$ and $St = 0.4$. Again, when $St = 0$, the composite approximation (41), represented by the dotted line in figure 6, is very accurate and it follows that the instantaneous mass transfer increases with the absolute value of the stagnation point location $|b(t)|$.

If $St = 0$ and if the stagnation point crosses the origin during the cycle, $b_1 > |b_0|$, $Sh(t)$ has two maxima per period, as can be seen in the left graphs in figure 6. The maxima will, in general, be unequal unless $b_0 = 0$ in which case the stagnation point oscillates symmetrically about the origin. The minimum mass flux occurs twice per period, when the stagnation point crosses the origin. Hence $Sh(t)$ appears similar to a 'rectified' harmonic oscillation with non-zero mean. Throughout most of the cycle the instantaneous Sherwood number is greater than the corresponding steady value (≈ 18.81); thus, the stagnation-point motion leads to a significant increase in time-averaged mass flux in this regime. Furthermore, an increase in b_1 will cause increases in the two maxima, while the minimum value of Sh remains the same. Hence, for $St = 0$ and $b_1 > |b_0|$, increasing b_1 causes a large increase in $\overline{Sh}$, see figure 7. Conversely, for large values of b_1, an increase in $|b_0|$ has only a modest effect on $\overline{\mathrm{Sh}}$

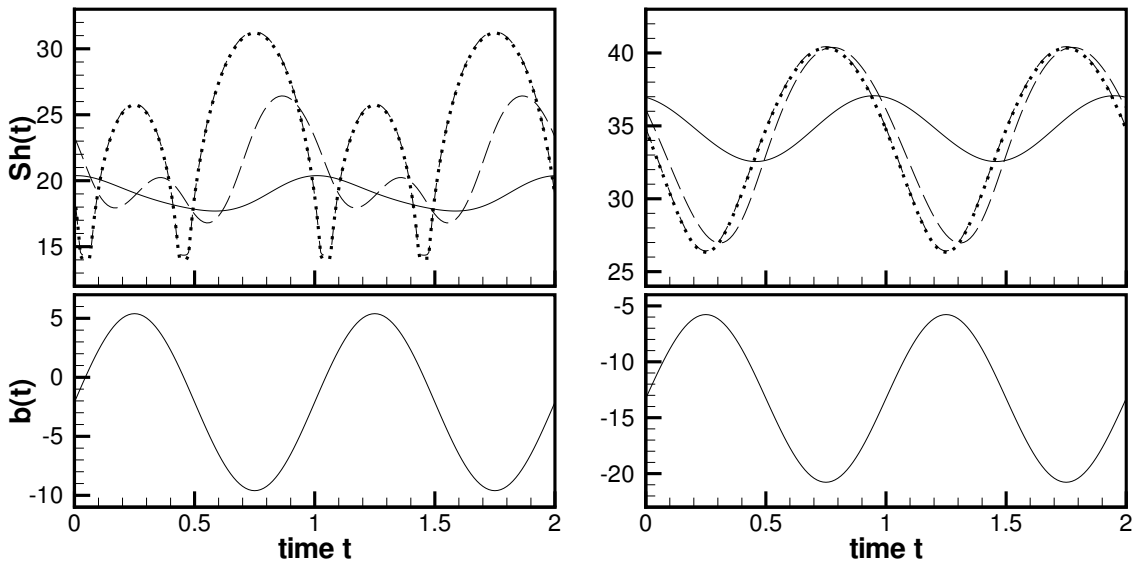

Figure 6. Upper graphs: Instantaneous mass transfer Sh(t) for a constant-strength stagnation point flow ($\alpha = 0$) undergoing positional oscillations about $b_0 = -2.1$ (left) and $b_0 = -13.28$ (right). $Pe_0 = 1500$, $b_1 = 7.5$. Short-dashed lines: $St = 0$; long-dashed lines: $St = 0.04$; solid lines: $St = 0.4$; dotted lines: quasi-steady approximation (41). Lower graphs: The corresponding position of the stagnation point, $b(t)$. Note the different scales on the vertical axes.

because the resulting increase in one maximum is approximately matched by the decrease in other, provided that b_1 remains greater than $|b_0|$.

If $|b_0| > b_1$, then the stagnation point never crosses the origin and there is only one maximum per period. In this case, moving the stagnation-point further from the origin causes a noticeable increase in $\overline{Sh}$. Indeed, figure 7 demonstrates that for a fixed b_1, the time-averaged mass flux is approximately independent of b_0, until $b_0 > b_1$ whereupon $\overline{Sh}$ begins to increase with b_0.

The above considerations all apply only to the quasi-steady results. If $St > 0$, "thermal" inertia again causes a decrease in the amplitude of the oscillations in $Sh(t)$ and introduces a phase lag between the extrema of mass flux and the extrema of the stagnation-point motion, equivalent to extrema of wall shear stress on the strip. As a result, the instantaneous (and thus also the time-averaged) mass flux remains much closer to the steady mass flux corresponding to the average stagnation point position. In fact, because $\alpha = 0$, the predictions of the large Strouhal number asymptotic analysis, (35) and (36), are identical to those of the quasi-steady approximation, (41).

Figures 6 and 7 show that the effects of "thermal" inertia already manifest themselves at a relatively small Strouhal number of $St = 0.04$. Furthermore, figure 7 demonstrates that at $St = 0.4$, the large Strouhal number analysis provides excellent predictions for the time-average mass flux $\overline{Sh}$. This is because the relative importance of "thermal" inertia is determined by the parameter $\chi \propto Pe_0^{1/3} St$, see equation (26), which is large even at relatively small values of St because $Pe_0 \gg 1$.

We, therefore, conclude that for moderate values of St, the time-average mass flux depends most strongly on the average position of the stagnation point with the amplitude of the positional oscillations having a much smaller effect.

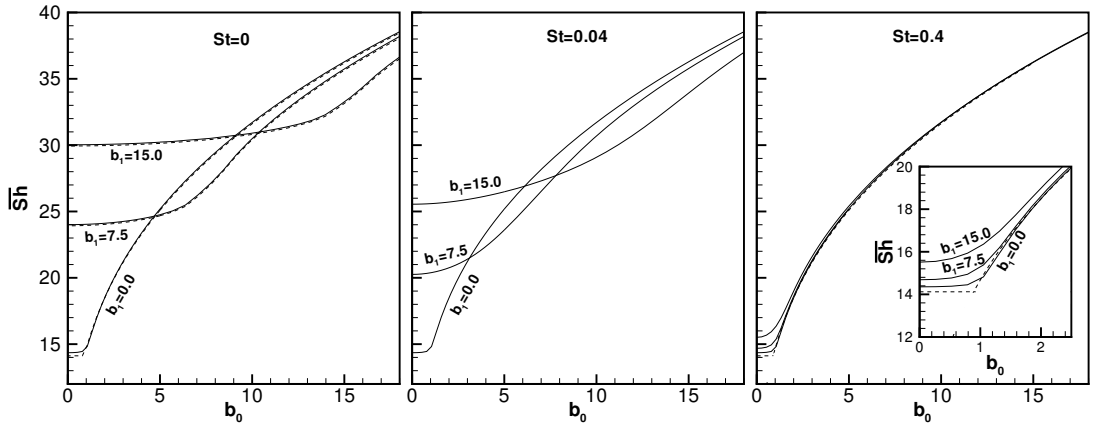

Figure 7. Average mass transfer $\overline{Sh}$ for a constant-strength stagnation point flow ($\alpha = 0$) undergoing positional oscillations. $b_1 = 7.5$, $\mathrm{Pe}_0 = 1500$. Solid lines: computational results; dashed lines: the average based on the quasi-steady approximation (41). When $\alpha = 0$, the predictions from the quasi-steady model are identical to those from the large Strouhal number analysis, (35) and (36).

5.2.3. *Flow pulsatility combined with stagnation point motion*

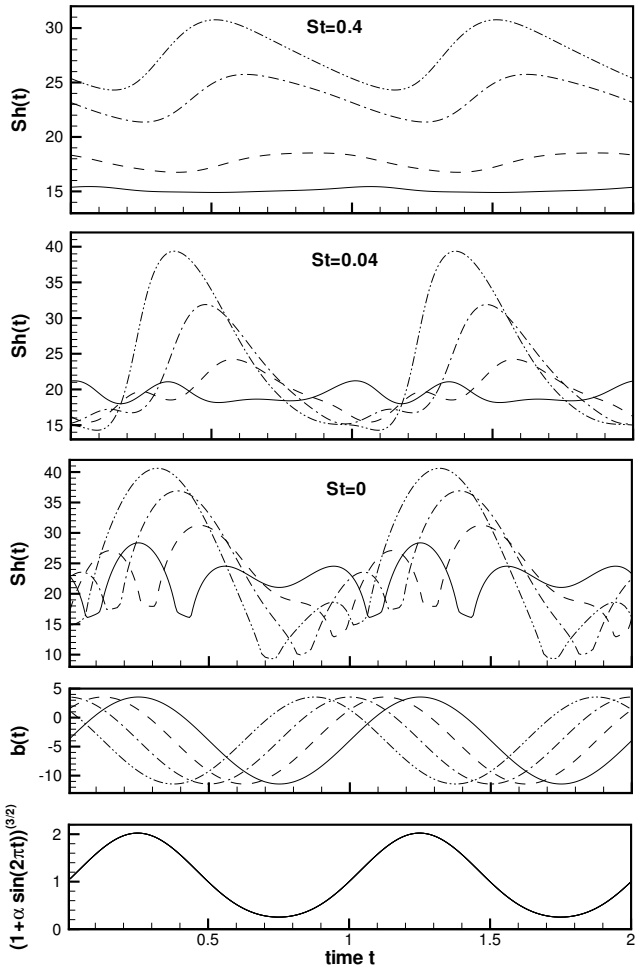

Figure 8. Instantaneous mass transfer $\mathrm{Sh}(t)$ for $St = 0,\ 0.04,\ 0.4$, stagnation point position $b(t)$ and strength of stagnation point flow for $\alpha = 0.6$, $b_0 = -3.95$, $b_1 = 7.5$ and $\mathrm{Pe}_0 = 1500$. Solid lines: $\phi = 0^o$; dashed lines: $\phi = 45^o$; dash-dotted lines: $\phi = 90^o$; dash-dot-dotted lines: $\phi = 135^o$.

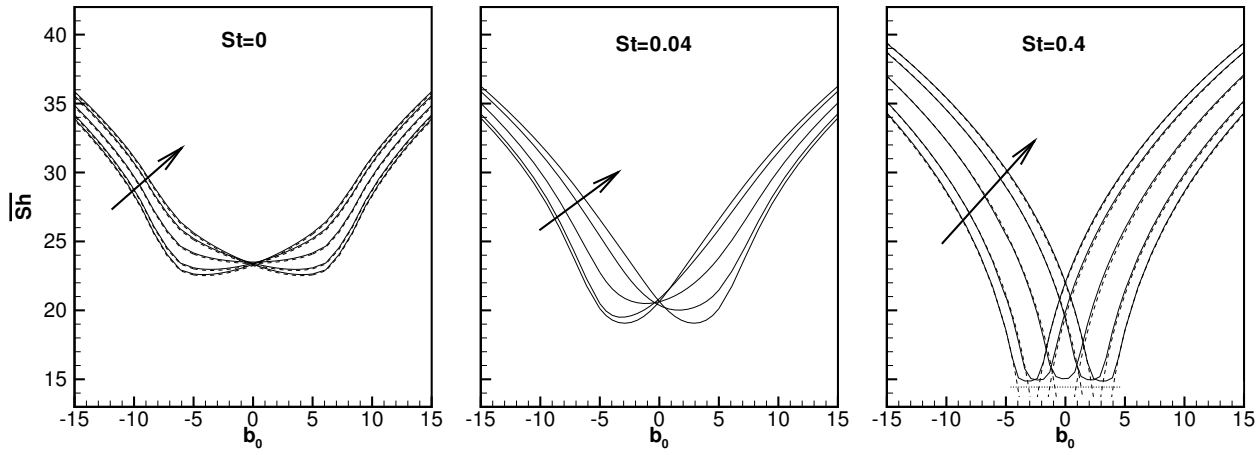

Figure 9. Average mass transfer $\overline{Sh}$ for $\alpha = 0.6$, $b_1 = 7.5$ and $Pe_0 = 1500$. Solid lines: computational results; dashed lines in graph for $St = 0$: average based on the quasi-steady approximation (41); broken lines in graph for $St = 0.4$: average based on the large Strouhal number approximations (35) and (36). $\phi = 0^o,\ 45^o,\ 90^o,\ 135^o$ and 180^o, increasing in the direction of the arrow.

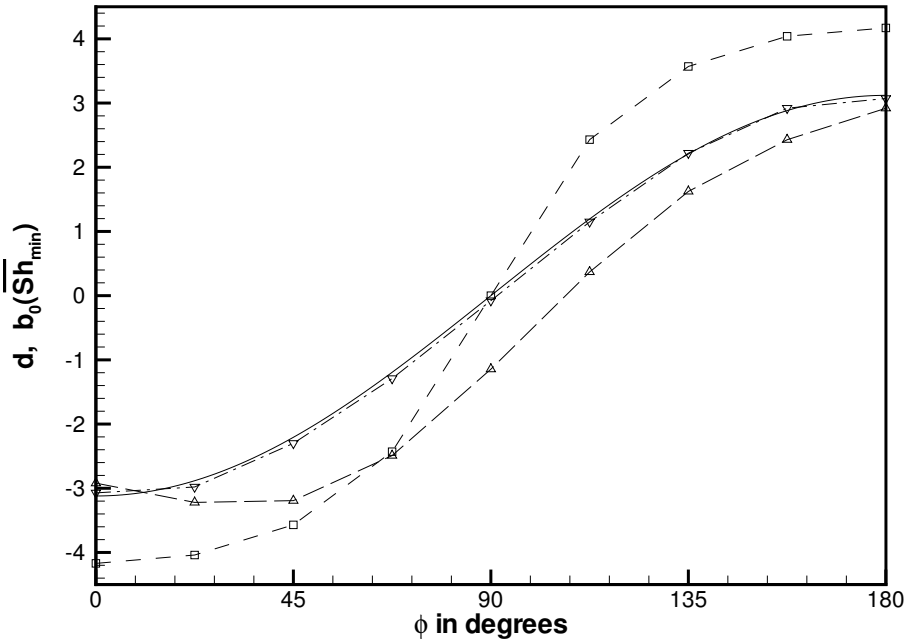

Figure 10. The distance of the centre of the positional oscillations from the point of zero mean wall shear stress, d, (solid line) and the average stagnation point position $b_0(\overline{Sh}_{min})$ for which the mass transfer is minimised (broken lines). Short-dashed line: $St = 0$; long-dashed line: $St = 0.04$; dash-dotted line: $St = 0.4$. $\alpha = 0.6$, $b_1 = 7.5$ and $Pe_0 = 1500$.

Finally, we consider the combined effects of flow pulsatility and stagnation-point motion, both $\alpha \neq 0$ and $b_1 \neq 0$. Figure 8 shows the instantaneous mass flux, $Sh(t)$, the stagnation-point location, $b(t)$ and the relative stagnation-point strength Pe/Pe_0 plotted against time for $St = 0,\ 0.04$ and 0.4. For $St = 0$ there is a local minimum in $Sh(t)$ when the stagnation point crosses the origin, c.f. §5.2.2. The value of the mass flux at this point is determined by the instantaneous strength of the stagnation-point flow and, therefore, depends crucially upon the phase difference, ϕ, between the two oscillations.

For the parameters used in figure 8, when $St = 0$ and $\phi = 0$, the fluctuations in mass flux are relatively small ($16.11 < \mathrm{Sh}(t) < 28.37$). At $\phi = 135^o$, the amplitude of the variations in mass flux ($9.41 < \mathrm{Sh}(t) < 40.62$) are about 2.5 times greater than for $\phi = 0^o$. In general, the amplitude of the variations in mass flux is greatest when the maximum velocity occurs at the maximum value of $|b(t)|$ and the amplitude is smallest when the minimum velocity occurs at that point. Furthermore, for a given average stagnation-point location, b_0, the time-average mass flux $\overline{Sh}$ is smallest if the phase angle, ϕ is such that the minimum incoming velocity occurs at the maximum of $|b|$ (when the stagnation point is furthest from the origin), see figure 9. Nonetheless, figure 9 demonstrates that, as in the case of pure positional oscillations, if $St = 0$, $\overline{\mathrm{Sh}}$ has only a weak dependence on the average position b_0 when $|b_0| < b_1$, but increases with b_0 once $|b_0| > b_1$. Note that $\overline{Sh}$ is symmetric in b_0 when $\phi = 90^o$ because in that case the incoming velocity has the same value at both the extreme stagnation-point positions.

Once again, the main effect of the "thermal" inertia introduced at finite Strouhal number is to limit the amplitude of the fluctuations in mass flux, see figure 8, and to introduce a phase lag into the mass flux relative to the position of the stagnation point. A consequence of the amplitude limitation is that for a given average stagnation-point location, b_0, the average mass flux, $\overline{Sh}$ becomes very sensitive to

the phase angle, see figure 9. Figure 9 also shows that, for finite values of the Strouhal number, there is a sharply-defined minimum in mass transfer, whose precise position depends upon ϕ.

At $St = 0.4$, the large Strouhal number analysis again provides an excellent approximation for $\overline{Sh}(b_0)$, despite the fact that, strictly speaking, the approximation breaks down when $b_1 > |b_0|$. It then follows from equation (35) that the minimum *mean mass transfer* might be expected to occur when $|\overline{\tau_{\rm av}}| = 0$, which is equivalent to $x_1^{\overline{\tau}=0} = 0$; see equation (17). Hence, we expect that the minimum *mean mass transfer* occurs when the centre of the strip is coincident with the point of zero *mean wall shear stress*.

This conjecture is examined in figure 10 in which the solid line shows the distance of the point of zero mean wall shear stress from the centre of the positional oscillations, $d = b_0 - x_1^{\overline{\tau}=0} = -b_1\mathcal{F}(\alpha)\cos(\phi)$ where $\mathcal{F}(\alpha) = 0.416$ for $\alpha = 0.6$. The broken lines show the average stagnation point position at which the mass transfer is minimised, $b_0(\overline{Sh}_{\rm min})$. At large values of the Strouhal number, d and $b_0(\overline{Sh}_{\rm min})$ coincide, indicating that at the minimum value of $\overline{Sh}$ we have $x_1^{\overline{\tau}=0} = 0$ and, as expected, the centre of the strip is located at the point of zero mean wall shear stress. This is in contrast to the quasi-steady predictions, where the minimum mean mass transfer can occur when the point of zero mean wall shear stress is located beyond the ends of the strip.

6. Summary and discussion

We have considered the mass transfer from a finite-length strip near a stagnation point that oscillates in both incoming velocity and location on a plane wall. The system is a highly idealised model of the mass transport that may occur when a short section of the arterial wall is damaged near regions of low wall shear stress. In particular, we wished to examine whether the location of the damaged region, relative to the time-average position of the stagnation point, would have any influence on the mass transport assuming a uniform (passive) cellular response to injury. Although the time history of the mass transfer can be very complex, we found that its time average is well-approximated by the asymptotic theories in the high and low frequency limits. In the physiologically relevant parameter regime, the fluid flow is still quasi-steady, yet the mass transfer displays genuine time-dependence and, indeed, the appropriate asymptotic limit is that of high frequency.

In general, the mass transfer from the arterial wall to the fluid increases with the Péclet number and is reduced in the vicinity of the stagnation point, as might be predicted from the steady and quasi-steady theories for heat transfer from a finite-length heated strip in a uniform shear flow (e.g. references [8,12]).

For physiologically realistic parameter values, corresponding to large Péclet and moderate Strouhal numbers, the oscillations in position and incoming velocity have a relatively weak effect on the time-averaged mass transfer when taken separately. In concert, however, the two oscillations can lead to a potent and strongly phase-dependent effect upon the time-averaged mass transfer from the strip. There is a sharply defined minimum in mass transfer when the centre of the strip is located at the point of zero mean wall shear stress. The exact location of this minimum is strongly dependent upon the phase difference, ϕ, between the two oscillations. Conversely, at very small values of the Strouhal number, the time-averaged mass transfer is largely insensitive to the phase difference and also to the location of the strip relative to the stagnation point, until the stagnation point no longer crosses the strip, at which point the mass transfer increases.

As $St \to \infty$, the mass transfer from the strip becomes completely time-independent. At $St = 0.4$, which represents the upper limit of the physiologically relevant parameter regime, the time course of the mass transfer still exhibits considerable oscillations.

The amplitude of these oscillations can vary significantly as a function of ϕ, again illustrating the importance of this parameter. The amplitude of the oscillations is smallest when the mean mass transfer is low, indicating that the mass transfer when the centre of the strip is located at the point of zero mean wall shear stress is approximately time-independent, as well as being strongly reduced. This finding lends further support to the notion that time-dependent effects may not be of direct importance in the development of arterial disease.

Although the model described in this paper is an extreme simplification of situation *in vivo* and applies only in the regions near stagnation points, the strong localisation effect is expected to carry through to three-dimensions and not to depend upon the precise details of the boundary conditions at the wall. It is therefore hoped that the analysis of our simplified model will aid the interpretation of data from numerical simulations in physiologically-realistic geometries.

The strong localisation effect may help to explain the focal nature of arterial disease and its correlation with regions of low wall shear stress. The low mass transfer from the wall in these regions will cause fewer circulating blood components to be activated and hence the time taken for the injury to be repaired will increase. If we assume that the arterial wall is regularly subject to minor damage, the slower repair time in regions of low wall shear stress could lead to a more rapid progression of arterial diseases in these regions. Furthermore, any chemicals secreted by the cells are likely to have more than one function. For example, platelet-activating factor has been shown to increase the vascular permeability and to cause changes in the cytoskeleton of cultured endothelial cells [13]. Thus, if the chemical concentration remains relatively high when the region of damage is near a stagnation point, the cell function could be significantly altered in these regions.

Throughout this paper, we have assumed that the cellular response is independent of the wall shear stress, a questionable assumption in the light of experimental evidence [5]. In their theoretical study, David *et al.* [14] found that it was necessary to include a shear-dependent reaction rate at the wall in order to reproduce experimental results for platelet deposition in stagnation-point flow. Indeed, it is possible that the stimulus for the "injury" to the cells is low wall shear stress itself. For example, the baseline permeability of endothelial cells *in vivo* has been shown to be inversely correlated with the time-averaged wall shear stress [15]. If this is the case, then the low-wall-shear stress stimulus coupled to the localisation effect described above will lead to a strong positive feedback mechanism and a highly focal biological response.

In conclusion, there is a significant and highly focal reduction in time-average mass transport when a chemical source, representing a short, damaged section of the arterial wall, coincides with the point of zero mean wall shear stress that occurs near an oscillating stagnation point. Thus, the focal nature of arterial disease may be in part explained by this localised mass transfer response, rather than any activity on the part of the endothelial cells. However, if the stimulus that causes the damage is itself low wall shear stress, the coupling of the stimulus to the localisation of the mass transfer response will lead to a more tightly focussed biological response than either mechanism acting alone.

Acknowledgements

Financial support from the EPSRC is gratefully acknowledged. The HSL2000 library routine MA42 was used in the numerical computations. ALH would like to thank T. J. Pedley for many helpful discussions during the early stages of this project.

References

1. C. G. Caro, J. M. FitzGerald, and R. C. Schroter: 'Atheroma and arterial wall shear: observation, correlation and proposal of a shear dependent mass transfer mechanism for atherogenesis'. *Proceedings of the Royal Society of London* **B 177**, (1971) 109–159.

2. M.H. Friedman, M. H. 'Atherosclerosis research using vascular flow models: from 2D branches to compliant replicas'. *ASME Journal of Biomechanical Engineering* **115** (1993) 595–601.

3. D.P. Giddens, C. K. Zarins, and S. Glagov: 'The role of fluid mechanics in the localization and detection of atherosclerosis'. *ASME Journal of Biomechanical Engineering* **115** (1993) 588–594.

4. A.L. Hazel and T. J. Pedley: 'Alteration of mean wall shear stress near an oscillating stagnation point'. *ASME Journal of Biomechanical Engineering* **120** (1998) 227–237.

5. P.F. Davies.: 'Flow-mediated endothelial mechanotransduction'. *Phys. Rev.* **75** (1995) 519–560.

6. G. Montrucchio, G. Alloatti, and G. Camussi: 'Role of platelet-activating factor in cardiovascular pathophysiology'. *Physiological Reviews* **80** (2000) 1669–1699.

7. F. M. White:, *Viscous Fluid Flow*. New York: McGraw-Hill, second edition (1991).

8. M.A. Lévêque, : 'Les lois de la transmission de chaleur par convection'. *Annales des Mines* **13 (Series 12)** (1928) 201–362.

9. T.J. Pedley: 'On the forced heat transfer from a hot film embedded in the wall in two-dimensional unsteady flow'. *Journal of Fluid Mechanics* **55** (1972) 329–357.

10. T.J. Pedley: *The fluid mechanics of large blood vessels*. Cambridge: Cambridge University Press (1980).

11. B.J. Folie and L. V. McIntire: 'Mathematical analysis of mural thrombogenesis'. *Biophysical Journal* **56** (1989) 1121–1141.

12. M.J. Lighthill: 'Contributions to the theory of heat transfer through a laminar boundary layer'. *Proc. Roy. Soc. Lond. A* **202** (1950) 359–377.

13. F. Bussolino, G. Camussi, M. Aglietta, P. Braquet, A. Bosia, G. Pescarmona, F. Sanavio, N. D'Urso, and P. C. Marchisio: 'Human endothelial cells are target for platelet-activating factor. I. Platelet-activating factor induces changes in cytoskeleton structures'. *Journal of Immunology* **139** (1987) 2439–2446.

14. T. David, S. Thomas, and P. G. Walker: 'Platelet deposition in stagnation point flow: an analytical and computational simulation'. *Medical Engineering and Physics* **23** (2001) 299–312.

15. M.H. Friedman, D. M. Grzybowski, A. L. Hazel, H. A. Himburg, and J. A. LaMack: 'Wall shear stress and albumin permeability at the porcine aortic trifurcation'. In: *Proceedings of the IVth World Congress of Biomechanics*. Madison, Wisconsin, USA, Omnipress (2002).